Journal of CO2 Utilization 63 (2022) 102125

Contents lists available at ScienceDirect

Journal of CO2 Utilization

journal homepage: www.elsevier.com/locate/jcou

Role of supercritical CO_2 impregnation variables on β-carotene loading into corn starch aerogel particles

Arthur Luiz Baião Dias [a], Tahmasb Hatami [b,*], Juliane Viganó [a,c], Erick Jarles Santos de Araújo [a], Lucia Helena Innocentini Mei [b], Camila Alves Rezende [d], Julian Martínez [a]

[a] Laboratory of High Pressure in Food Engineering, School of Food Engineering, University of Campinas, UNICAMP, 13083-862 Campinas, SP, Brazil
[b] Department of Materials Engineering and Bioprocess, School of Chemical Engineering, University of Campinas, UNICAMP, 13083-852 Campinas, SP, Brazil
[c] Centro de Ciências da Natureza, Universidade Federal de São Carlos, Rod. Lauri Simões de Barros, km 12 – SP 189, Buri, SP 18290-000, Brazil
[d] Institute of Chemistry, University of Campinas, UNICAMP, 13083-970 Campinas, SP, Brazil

ARTICLE INFO

Keywords:
Supercritical fluid impregnation
Corn starch aerogel
β-carotene

ABSTRACT

β-carotene is a natural dye with antioxidant and provitamin A activities, which has essential roles in human health. However, its direct use in food products is unviable since it is susceptible to oxidation, easily isomerization under light, heat or acids, and has low water solubility and oral bioavailability. To address this issue, this work reports, for the first time, the impregnation of β-carotene into corn starch aerogels using supercritical carbon dioxide (sc-CO_2). The aerogel particles were produced by the emulsion-gelation method, dried by sc-CO_2 and loaded with β-carotene by sc-CO_2 impregnation. The impacts of pressure (15 and 30 MPa), temperature (40 and 60 °C), average depressurization rate (0.25–2.61 MPa/min), and cycles (1−4) were investigated on loading. Excepting depressurization rate, all variables played fundamental roles in loading, reaching a maximum of 0.96 mg β-carotene/g aerogel (30 MPa, 40 °C, 0.40 MPa/min, four cycles).

1. Introduction

β-carotene is a natural dye with bioactive attributes such as antioxidant and provitamin A activities. However, it is susceptible to oxidation due to the presence of unsaturated compounds in its structure, and it is easily isomerized when exposed to light, heat, and acids. Low oral bioavailability, low water solubility and high melting point of β-carotene also compromise its use in food systems, especially in high humidity products (beverages, sauces, and desserts) [1]. Therefore, several techniques have emerged to enhance the stability and functionality of poorly water-soluble dyes, like β-carotene, by synthesizing delivery systems such as nanoemulsions, solid lipid nanoparticles [2–5], and supercritical impregnated aerogels [6].

Aerogels are solid materials with high porosity and surface area, produced by replacing the liquid in a gel with gas while keeping the gel structure unchanged. Recently, aerogels fabricated from natural polymers (bioaerogels) have been highlighted due to their bioavailability, safety, and biodegradability [7]. Considering food industries, starch is a promising and suitable alternative for aerogel formulation as it is cheap and generally recognized as a safe (GRAS) [8–13]. Starch aerogels can be obtained from several sources, namely, potatoes, corn, cassava, peas, among others. Chemically, starch macromolecules are formed by two main components, amylose and amylopectin, which are alternately arranged to create a semi-crystalline structure. Amylose has a linear structure, while amylopectin is highly-branched, with a relative proportion of these components varying depending on the starch source [14–16]. Three main steps are described in the production of starch aerogels: (1) hydrogel formation based on gelatinization and retrogradation properties, (2) water replacement in the gel structure with an appropriate organic solvent such as ethanol, and (3) removal of the alcoholic phase using supercritical CO_2 (sc-CO_2) drying [17,18]. The use of starch in the synthesis of aerogels allows creating solid networks with different geometric shapes, such as monoliths, microspheres and microparticles. Starch aerogels in form of microparticles are highly recommended when the objective is the incorporation of target compounds, such as β-carotene, which stands out for its bioactivity and wide distribution in the nature [19,20].

Supercritical impregnation is an environmentally sustainable process that uses CO_2 as a mean to incorporate active agents into solid materials through interactions, such as Van der Waals or hydrogen bindings,

* Corresponding author.
E-mail address: thatami@unicamp.br (T. Hatami).

https://doi.org/10.1016/j.jcou.2022.102125
Received 28 April 2022; Received in revised form 14 June 2022; Accepted 3 July 2022

between functional groups of an active substance and polymer, or physical entrapment due to the depressurization step [21–24]. This technique is able to impregnate solid matrices with high efficiency and without requiring toxic solvents, under high diffusion coefficient, and mild supercritical conditions [19,25–27]. It has been widely reported in the literature that the impregnation of hydrophilic aerogels (such as starch aerogels) with poorly water-soluble drug enhances the drug solubility in water [28,29]. The reason is that once the impregnated aerogel is subjected to aqueous solution, the carrier is dissolved and the drug is released in the form of small colloidal particles with high specific surface area, which therefore causes higher dissolution rate of the drug [30]. The impregnation of starch aerogels can also enhance the controlled release of β-carotene in foods and nutraceuticals. One of the main challenges in supercritical impregnation is finding the best process conditions for efficient impregnation without changing the physical properties of structured matrices, such as aerogels. Literature presents several hundred works on the use of this technique for the carriage of polymers with medicines [31], food packaging [32–37], and functional compounds in pharmaceutical materials [38]. sc-CO_2 was used to impregnate α-tocopherol and menadione in a maize starch aerogel [39]. The maximum impregnation for both components was obtained under 15 MPa and 60 °C, which was 19.99 wt% for α-tocopherol and 8.76 wt% for menadione. In another relevant work, a one-pot process was developed to fabricate starch aerogel and to impregnate it with green coffee oil [40]. The highest impregnation yield (39 wt%) was obtained under 30 MPa and 40 °C for 12 h.

Few works applied sc-CO_2 impregnation in aerogels, and to the best of our knowledge, there are no works reporting the production of corn starch aerogel impregnated with β-carotene. Thus, the main objective of the presented work was to evaluate the effect of process variables (e.g. pressure, temperature, depressurization rate, and the number of impregnation cycles) on the β-carotene loading in corn starch aerogels using sc-CO_2, as well as the morphological and physico-chemical properties of the aerogel.

2. Material and methods

2.1. Materials

Corn starch was kindly donated by Ingredion Ing. Ind. Ltda. (São Paulo, Brazil), commercial soybean oil (Soya, Bunge Brazil) was purchased in a local market (Campinas, Brazil), and Span® 80 was acquired from Sigma-Aldrich (St. Louis, USA). Absolute ethanol (≥99.5%, v/v) and carbon dioxide (≥99.0%) were, respectively, purchased from Synth (Diadema, Brazil) and White Martins (Campinas, Brazil). β-carotene standard (≥93.0%) was purchased from Merck Group (Darmstadt, Germany) and petroleum ether was acquired from Synth (Diadema, Brazil).

2.2. Synthesis of corn starch aerogels

Hydrogel particles were synthesized as reported by De Marco et al. [41], with some modifications. A corn starch solution (15 wt%) (solution A) was prepared by diluting solid corn starch into deionized water and magnetically stirring at 200 rpm and room temperature for 15 min. In parallel, the soybean oil containing 2 wt% Span® 80 (solution B) was prepared and mechanically stirred (600 rpm) in a beaker (500 mL; 7.4 cm internal diameter) placed inside a heating bath at 75 °C. Then, solution B was slowly poured into solution A at 600 rpm. The mass ratio between solutions A and B was 1:3, totalizing 280 g. Agitation was carried out during the first 60 min and then the emulsion was kept at rest in the heating bath for another 2 h, completing 3 h. Afterwards, the emulsion was stored under refrigeration (4 °C) for 72 h to allow the corn starch hydrogel retrogradation. Next, 500 mL of ethanol/water (30 vol %) were added into the gelled emulsion and the final mixture was transferred to a funnel to separate the hydroalcoholic phase containing the hydrogel particles from the oily phase. Then, particles were separated from the liquid through a filter paper (vacuum filtration) and followed to solvent exchange.

The filtered particles were immersed into ethanol/water solutions of 30:70, 60:40, 90:10 and 99.5:0 (vol%). The solvent was exchanged every 24 h and three exchanges were performed at 99.5 vol% ethanol. The particle-to-liquid mass ratio was 1:5, and the alcogel particles were kept at 99.5 vol% ethanol until sc-CO_2 drying.

Fig. 1(a) shows the flowsheet of the sc-CO_2 unit for both drying and impregnation, consisting of block valves (Autoclave Engineers, Erie, USA), micrometer valve (Autoclave Engineers, Erie, USA), cooling bath (Marconi, S.A., Campinas, Brazil), CO_2 pump (Maximator, Zorge, Germany), heating bath (Marconi, S.A., Campinas, Brazil), manometers (Zurich, São Paulo, Brazil), thermocouples, and a 100.0 mL stainless-steel vessel. For clarification, Fig. 1(b) shows the configuration of the cell in the sc-CO_2 unit for drying in more detail. In a typical experiment for sc-CO_2 drying, firstly, approximately 25.0 g of the alcogel particles were placed into a paper bag and transferred to a 54.37 mL stainless-steel vessel. The vessel was closed and heated at 40.0 ± 1.0 °C. The system was pressurized with sc-CO_2 to reach 12.0 ± 0.5 MPa, and the drying vessel was kept at this pressure and temperature for 5 min (static time). The CO_2 flow rate was adjusted at 10.0 g/min and the process was completed when the S/F (mass ratio between the consumed CO_2 and alcogel particle) reached 25. Experimental conditions were based on Hatami et al. [42], who performed the sc-CO_2 drying of alginate-based aerogel particles. Finally, depressurization was carried out at 1.5 MPa/min and constant temperature (40 °C) until the atmospheric pressure was reached. The particles were removed from the drying vessel and stored in a desiccator until impregnation. Several batches of hydrogel production and sc-CO_2 drying were performed to achieve the required aerogel amount for further steps of supercritical impregnation and aerogel characterization. The total mass of aerogel produced was homogenized to reach a uniform batch.

2.3. Supercritical impregnation

Fig. 1(c) shows the configuration of the drying cell in the sc-CO_2 unit for impregnation of β-carotene in corn starch aerogels. In a typical experiment for one cycle sc-CO2 impregnation, firstly, the β-carotene standard was diluted (10 mg/mL) in ethanol. Next, approximately 1.0 g of corn starch aerogels was added in an 18.70 mL glass beaker (2.3 cm internal diameter) and inserted into the 100.0 mL stainless-steel vessel. Then, 2.0 mL of the β-carotene solution was pipetted into the vessel keeping it outside the glass beaker. A cotton layer was added to the top of the glass beaker to avoid particle loss during depressurization. The vessel was closed, and the system was heated and pressurized at the desired operational conditions. The static time of impregnation was 60 min, and after that, the vessel was depressurized by venting out sc-CO_2 at constant flow rate. This 60 min is twice the contact time required to saturate supercritical CO_2 with β-carotene using a single-pass flow apparatus [43]. About two cycle sc-CO2 impregnation, 1.0 g of the impregnated corn starch aerogels with β-carotene from the first cycle was put inside the stainless-steel vessel under the same operating conditions for 60 min, and then, sc-CO_2 was vented out at same flow rate. This procedure was exactly repeated for the third and fourth cycle, as well.

Effects of the system depressurization rate (0.25–2.61 MPa/min), pressure (15 – 30 MPa) and temperature (40 – 60 °C) during the static impregnation, and the number of cycles (1−4) were evaluated on the sc-CO_2 impregnation of β-carotene in corn starch aerogels. All experiments were performed in duplicate and the impregnated particles were stored in the dark at −18 °C for further characterization.

2.3.1. Loading of β-carotene

Approximately 50.0 mg of impregnated corn starch aerogels were weighed, mixed with 1.0 mL petroleum ether, vortexed, and filtered

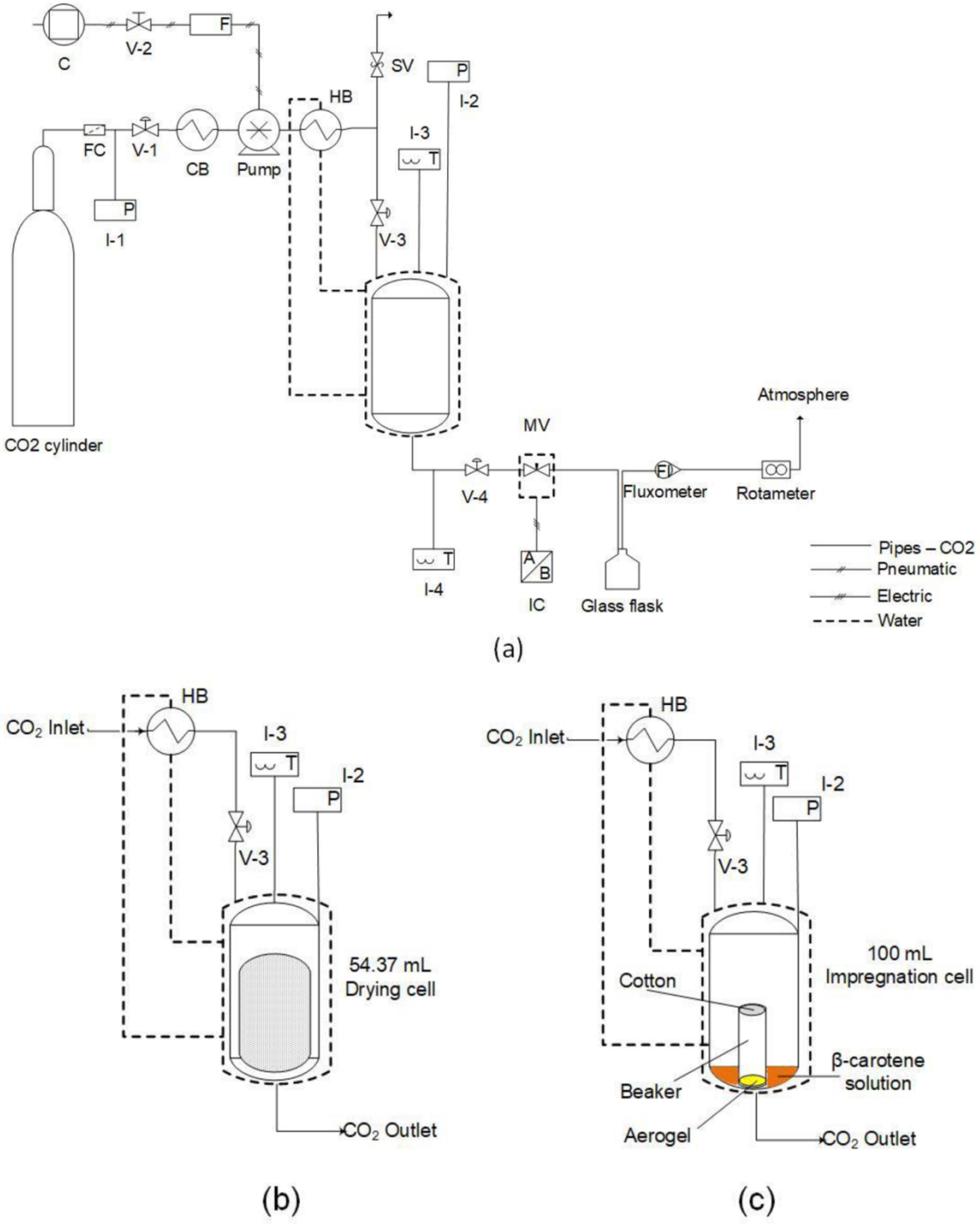

Fig. 1. Flowchart of (a) sc-CO_2 unit, (b) the configuration of cell in the sc-CO_2 unit for drying, and (c) the configuration of cell in the sc-CO_2 unit for impregnation. V-1 to V-4: block valves; MV: micrometer valve; SV: safety valve; C: compressor; F: air filter; FC: CO_2 filter; CB: cooling bath; HB: heating bath; I-1 and I-2: pressure indicators; I-3 and I-4: temperature indicators; IC: temperature controller.

(Chormafil Xtra PA-20/25, Macherey-Nagel, Düren, Germany) to desorb the β-carotene from the particles. The β-carotene content impregnated in the corn starch aerogel particles was determined by spectrophotometry at 450 nm using a FLUOstar Omega microplate reader (BMG LABTECH GmbH, Ortenberg, Germany) with Omega Mars 3.32R5 data analysis software. The quantification followed the methodology developed by Rodriguez-Amaya [4] using a β-carotene standard curve ($y = 0.1075x + 4.0 \times 10^{-5}$, $R^2 = 0.9942$). The β-carotene loading was determined using Eq. (1), in which $m_{(\beta-carotene)}$ is the mass (mg) of loaded β-carotene and $m_{aerogel}$ is the mass (g) of impregnated corn starch aerogel.

$$Loading_{(\beta-carotene)}(\mathrm{mg}/\mathrm{g}) = \frac{m_{(\beta-carotene)}}{m_{(aerogel)}} \quad (1)$$

2.4. Chemical and physical analyses

2.4.1. Particle size distribution

The particle size distribution of the corn starch aerogel particles was determined using a Laser Diffraction Particle Size Analyzer Mastersizer (Mastersizer 3000 - MAZ3000; Malvern Instruments, Worcestershire,

UK). Ethanol (99.5%) was used as dispersant agent, keeping the stirrer speed at 1750 rpm. An optical microscope (Leica – DMLM, Cambridge, UK) was used to determine aerogel particle size. A minimum of 20 images were obtained under incident light mode or dark field, to assure data reproducibility. The volume-surface mean diameter (D_{32}) and volume mean diameter (D_{43}) of the particles were determined according to Eq. (2) and Eq. (3), respectively.

$$D_{32} = \frac{\sum n_i \quad d_i^3}{\sum n_i \quad d_i^2} \tag{2}$$

$$D_{43} = \frac{\sum n_i \quad d_i^4}{\sum n_i d_i^3} \tag{3}$$

Where n_i is the number of aerogel particles with diameter d_i.

The polydispersity (*PSD*) and the width distribution (*Span*) of the particles were determined according to Eq. (4) and Eq. (5), respectively.

$$\text{PSD} = \frac{d_{(90)}}{d_{(10)}} \tag{4}$$

$$\text{Span} = \frac{d_{(90)} - \quad d_{(10)}}{d_{(50)}} \tag{5}$$

Where $d_{(90)}$, $d_{(50)}$ and $d_{(10)}$ are the equivalent volume diameters at 90%, 50%, and 10% of the cumulative volume of particles, respectively.

The volume density (*VD*) data of particles against the size particles was then fit to a Gaussian three parameters equation (Eq. (6)):

$$VD = A \times exp\left(- \left(\frac{\ln d_p - B}{C} \right)^2 \right) \tag{6}$$

Where d_p is the particle diameter (μm), and *A*, *B*, and *C* are dimensionless constants. The accuracy of Eq. (6) is evaluated using the Root-Mean-Square-Error (*RMSE*) as follows:

$$RMSE = \sqrt{\frac{\sum_{i=1}^{N} (V_{Di} - \quad V_{D(i-1)})^2}{N}} \tag{7}$$

Where V_{Di} and $V_{D(i-1)}$ are the volume density of the particle size *i* and *i* – 1, respectively, and *N* is the total number of particle sizes measured.

2.4.2. Nitrogen adsorption-desorption measurements

Nitrogen adsorption-desorption measurements were applied to determine the surface area, total pore diameter, and total pore volume of crude corn starch, and corn starch aerogels before and after β-carotene impregnation. Approximately 100.0 mg of the samples were weighed and heated at 60 °C under vacuum (< 1 MPa) for 15 h. The adsorption-desorption isotherms of nitrogen were obtained at − 195.85 °C (Quantachrome Instruments, Nova2200e). The multipoint Brunauer–Emmett–Teller (BET) model was used to determine the surface area of the samples in the relative pressure range of 0.07–0.30 (*P/Po*). The Barret-Joyner-Halenda (BJH) model was applied to calculate the total pore diameter and total pore volume of the samples using a desorption isotherm for a relative pressure below 0.95.

2.4.3. Scanning electron microscopy (SEM)

A scanning electron microscope (SEM) (LEO Electron Microscopy, Leo 440i, Cambridge, England) with secondary electron detector was used to analyze the microstructures of the impregnated corn starch aerogels particles. Before imaging, samples were gold-sputtered to reduce charging effects at 50 pA for 2 min (EMITECH, K450, Kent, UK). To guarantee the reproducibility of the results, a minimum of 20 images were obtained for each sample. The analysis of the particles was performed under vacuum using an acceleration tension of 15 kV.

2.4.4. Differential scanning calorimetry (DSC)

Differential scanning calorimetry (DSC) was used as a thermo-analytical technique to measure the phase transitions of aerogels before and after β-carotene impregnation. A HP DSC1 (Mettler Toledo, Schwerzenbach, Switzerland) was employed. Samples were weighed into a 40.0 μL aluminum pan, and the curves were plotted from 25° to 300°C with a heating rate of 10 °C/min. Nitrogen was used at a flow rate of 50 mL/min.

2.4.5. X-ray diffraction (XRD) analysis

XRD analysis was used to investigate the crystallinity and structure of crude corn starch, corn starch aerogel, and impregnated corn starch aerogel. X-ray diffraction analysis (Philips Analytical X-Ray, X'Pert-MPD, Almelo, Netherlands) of the aerogels before and after β-carotene impregnation were performed using a position-sensitive detector and CuKα radiation. Diffraction was measured within the 10–60° range, with a step size of 0.037°, and counting a time of 2 s per step.

2.4.6. Fourier transform infrared spectroscopy (FTIR)

FTIR analysis evaluates possible chemical changes in the structure of the samples before and after the drying and adsorption processes. FTIR was conducted in an infrared spectrophotometer (model IRPrestige-21, Shimadzu, Kyoto, Japan) with a resolution range from 400 to 4000 cm^{-1}. Approximately 3.0 mg of samples were mixed with 200.0 mg of KBr. The mixture was macerated in grail and agate pistil and then transferred to a 13.0 mm diameter stainless steel mold and pressed in a hydraulic press (Shimadzu, SSP-10A, Kyoto, Japan) connected to a vacuum pump. Force of 80 kN was applied for 10 min under vacuum to form the tablet. Data acquisition was made by Software IRSolution, version 1.60. The IR spectra normalization was carried out through the ratio between the spectral intensity and the square root of the sum of squares intensities of the respective spectrum, as shown in Eq. (8) [44,45]:

$$SN_{i,j} = \frac{S_{i,j}}{\sqrt{\sum_{j=}^{n} {}_1 (S_{i,j})^2}} j = 1, 2, 3, ..., \text{n} \tag{8}$$

Where SN_i is the normalized spectral absorbance of sample *i* at the *j*th wavenumber, $S_{i,j}$ is the spectral absorbance of sample *i* at the *j*th wavenumber and *n* is the number of wavenumbers in the scanning spectral region.

2.5. Statistical analyses

The results were statistically evaluated by one-way analysis of variance (ANOVA), through the Tukey's test at the level of 5% ($p \leq 0.05$). Tukey's test was measured using the software MINITAB® (Release 16.1.0, Minitab Inc.).

3. Results and discussion

3.1. Effects of depressurization rate, pressure, temperature and number of cycles on β-carotene loading

The effect of average depressurization rate (0.45 and 2.61 MPa/min) on the loading of β-carotene in corn starch aerogels was evaluated at 30 MPa and 60 °C. The average depressurization rates of 0.45 and 2.61 MPa/min were obtained by releasing the CO_2 inside the vessel at constant flow rates of 1.79 and 10.43 g CO_2/min, respectively. For better comprehension, Fig. 2 represents the exact pressure profile along the depressurization under two CO_2 flow rates. These profiles, which are nonlinear, were calculated in two steps by the assumption of constant temperature: in the first step, the instantaneous CO_2 density during the depressurization was calculated by dividing the instantaneous mass of CO_2 remaining inside the vessel by the total active volume of the vessel,

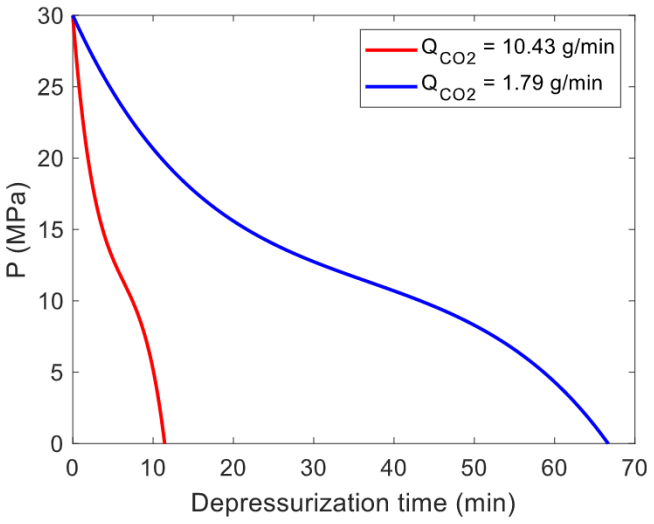

Fig. 2. Pressure profiles along the depressurization at 60 °C.

and in the second step, the pressure inside the vessel was obtained using the Peng-Robinson Equation of State with the known values of density and temperature. Based on Fig. 2, the pressure profiles, particularly for CO_2 flow rate of 10.43 g CO_2/min, drop substantially at the early time of depressurization, then decrease with lower but still high slope, and decline significantly again at the end of depressurization time.

The loading of β-carotene did not present statistical difference between both depressurization rates ($p > 0.05$), achieving 0.22 ± 0.05 and 0.22 ± 0.04 mg β-carotene/g aerogel for 0.45 and 2.61 MPa/min, respectively. Other works observed similar behaviors: the impregnation of terpenoketones (thymoquinone and R-(+) -pulegone) in low density polyethylene (LDPE)/sepiolite nanocomposites [46] and impregnation of LDPE films with a mixture of two terpenic ketones (thymoquinone and R-(+) -pulegone) [47] were not significantly influenced by the depressurization rate. Thus, focusing on the time required to depressurize the system, the CO_2 flow rate along depressurization was set constant at 1.79 g CO_2/min in the following steps of this work, and the associated depressurization rate for each run was calculated using the initial pressure and temperature.

Table 1 presents the effects of pressure (15 and 30 MPa) and temperature (40 and 60 °C) on the β-carotene loading in corn starch aerogels using sc-CO_2 impregnation. At both isotherms, the loading increased with pressure. Particularly, a pressure increase from 15 to 30 MPa at 40 °C raised the impregnation from 0.01 to 0.37 mg β-carotene/g aerogel. However, temperature had opposite effects at lower and higher pressures. The increase in temperature from 40 to 60 °C, at 15 MPa, increased the loading from 0.01 to 0.15 mg β-carotene/g aerogel; and at 30 MPa, the loading decreased from 0.37 to 0.22 mg β-carotene/g aerogel. The combination of pressure at 30 MPa and temperature at 40 °C provided the highest β-carotene loading (0.37 mg β-carotene/g aerogel). Therefore, this condition was adopted to evaluate the number of cycles of sc-CO_2 impregnation.

Table 1
Effects of pressure and temperature on the loading of β-carotene in corn starch aerogels using sc-CO_2 impregnation.

P (MPa)	T (°C)	Average depressurization rate (MPa/min)	Number of cycles	Loading (mg β-carotene/g aerogel)
15	40	0.25	1	0.01 ± 0.01^{c}
15	60	0.33	1	0.15 ± 0.03^{bc}
30	40	0.40	1	0.37 ± 0.10^{a}
30	60	0.45	1	0.22 ± 0.05^{ab}
30	40	0.40	1	0.37 ± 0.10^{C}
30	40	0.40	2	0.65 ± 0.04^{B}
30	40	0.40	3	0.90 ± 0.16^{A}
30	40	0.40	4	0.96 ± 0.07^{A}

*Same lowercase and uppercase letters in the same column indicate no statistical difference ($p < 0.05$).

The effect of temperature and pressure during sc-CO_2 impregnation is well discussed in the literature [24,48]. According to Carvalho et al. [48], the adsorption and precipitation processes performed under sc-CO_2 are impacted by the dissolution of the target compound in the supercritical mixture (in the case of this work, β-carotene + sc-CO_2), by the mass transfer from the bulk mixture to the solid material surface, and by depressurization. To clarify the role of temperature and pressure on the loading, it is required to first illustrate the roles of these two parameters on the solubility of β-carotene in sc-CO_2, CO_2 sorption and polymer (starch) swelling, and the interaction between β-carotene and the polymer [24].

Regarding the solubility of β-carotene in sc-CO_2, Fig. 3 represents the impacts of pressure on the solubility at 40 and 60 °C. The solubility data for the pressure smaller than 20 MPa was taken from the work conducted by Mendes et al. [43], and the data for the pressure equal to or higher than 20 MPa was obtained from the research performed by Johannsen and Brunner [49]. For both isotherms, the solubility increases with pressure, which is related to the increase of CO_2 density with pressure. Unlike pressure, increasing the temperature influences the solubility in two different ways: it increases the vapor-pressure of β-carotene [50], which has a positive impact on the solubility, and it decreases the CO_2 density, which has a negative impact on the solubility [24]. Referring to Fig. 3, the solubility, for pressure below 16 MPa, decreases slightly as temperature increases from 40 to 60 °C, while the solubility, for pressures above 16 MPa, increases substantially with temperature. This particular pressure (16 MPa), which corresponds to the change of the influence of temperature on the solubility, is known as the crossover pressure. It can be inferred from Fig. 3 that the vapor pressure of β-carotene is the dominant factor above the crossover pressure, whereas CO_2 density is the leading factor below the crossover pressure.

Regarding the CO_2 sorption and polymer swelling, both increase with pressure [24,51,52]. Unlike pressure, the impact of temperature is particularly complex for semicrystalline polymers like starch, and it depends on the glass transition temperature (T_g) and melting temperature of the polymer (T_m) at the system pressure [24]. For temperatures below T_g, the change in structural properties of polymer is limited, whereas for temperatures above T_g, the increase in temperature has two opposite effects [24]: (1) it enhances chain mobility that consequently

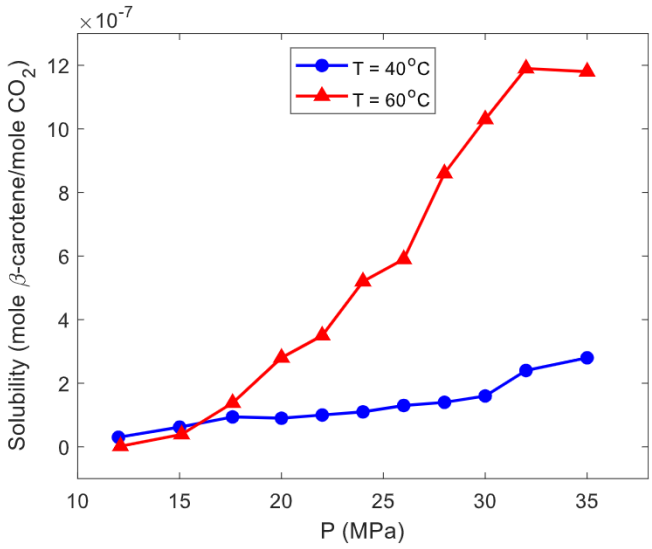

Fig. 3. Solubility of β-carotene in supercritical CO_2 [43,49].

improves both CO_2 sorption and polymer swelling, and (2) it decreases CO_2 density and causes recrystallization in semicrystalline polymers that leads to the reduction of CO_2 sorption and polymer swelling. As temperature increases toward T_m, the crystal regions of the polymer melts that increases the CO_2 sorption and polymer swelling due to the increasing the amorphous parts in the polymer [53].

Referring to the interaction between β-carotene and the polymer, there is still no study in the literature about the role of temperature and pressure on this interaction under supercritical condition. Nevertheless, as a general rule, the higher interaction between drug (β-carotene) and polymer (starch) increases the impregnation performance [24]. β-carotene and starch interact mostly through H+ bonding (inter and intra-helical) and CH–π stacking (alkene chains - glucose rings), and the interaction is controlled by non-covalent forces [54].

According to the aforementioned roles of temperature and pressure on the solubility of β-carotene in sc-CO_2, CO_2 sorption and polymer swelling, and the interaction between β-carotene and the polymer, it is now possible to analyze the role of temperature and pressure on the loading yield. The positive impact of increasing pressure, at both isotherms, on the impregnation yield in Table 1 is due to the simultaneous increasing of the solubility of β-carotene in sc-CO_2, the CO_2 sorption, and the polymer swelling. Moreover, though increasing temperature from 40 to 60 °C, at 15 MPa, does not have a considerable impact on the solubility of β-carotene in sc-CO_2, it enhances impregnation yield (Table 1) by raising the chain mobility of the polymer. At 35 MPa, although the same increasing in temperature increases the solubility of β-carotene in sc-CO_2 considerably (Fig. 3), the reduction of impregnation yield in Table 1 is probably related to the weakening of the bonds between β-carotene and starch with temperature.

Table 1 also provides the effects of the number of pressurization/depressurization cycles (1−4) of sc-CO_2 impregnation on the β-carotene loading. The increase in the number of cycles from 1 to 2 raised the loading by 0.25 mg β-carotene/g aerogel; a further increase from 2 to 3 cycles raised the loading by the same amount (0.25 mg β-carotene/g aerogel); finally, the increase from 3 to 4 cycles had smaller impact on the yield and increased it by only 0.06 mg β-carotene/g aerogel. The first possible reason for this trend is the decrease of free active surface on the aerogel in the last cycle. The second possible reason is that the loading of β-carotene in three first cycles leads to the obstruction of the external pores of the particle surface, thus hampering the diffusion of supercritical solution (β-carotene + sc-CO_2) from the bulk to the intra particle during the fourth cycle, which consequently weakens the loading in the last cycle compared to the previous cycles.

3.2. Physicochemical evaluation of corn starch aerogels

Fig. 4 presents the particle size distribution of corn starch aerogels produced by sc-CO_2 drying (12 MPa, 40 °C, and CO_2 flow rate of 10 g/min) provided by laser diffraction and fitted by Eq. (6), and their optical microscopy image. Fig. 4(a) is obtained using many optical microscopy images, one of which is represented in Fig. 4(b). As shown in Fig. 4(a), Eq. (6) fits well to the volume density with R-square of 0.9938, and RMSE pf 0.1977. The calculated constants of Eq. (6) are 10.69 for *A*, 3.057 for *B*, and 0.6372 for *C*. Based on Fig. 4(a), corn starch aerogels with highly uniform size were produced. Further analysis of this figure shows that the volume-surface mean diameter (D_{32}) and the volume mean diameter (D_{43}) of the aerogel particles are 10.5 and 20.5 μm, respectively, and their polydispersity (*PSD*) and the width distribution (*Span*) are 1.32 and 3.73, respectively. Microparticles obtained in this work can be classified based on the Merkus classification [55] as medium particles (10–1000 μm). Fig. 4(a) shows that the particle diameter distribution is mostly between 50 and 100 μm. This may be due to two reasons; firstly, larger particles are agglomerates of particles, as shown later in Fig. 9, and secondly, smaller particles are removed by the liquid solvent in the solvent exchange process and the supercritical fluid in the drying process.

Fig. 5 shows the nitrogen adsorption-desorption measurements of crude corn starch (Fig. 5(a)), corn starch aerogels produced by sc-CO_2 drying (12 MPa, 40 °C, and CO_2 flow rate at 10 g/min) (Fig. 5(b)), and sc-CO_2 impregnation (30 MPa, 40 °C, average depressurization rate at 0.40 MPa/min, and 4 cycles) (Fig. 5(c)). Based on the adsorption isotherms in the IUPAC classification presented by Yahia et al. [56], the isotherms in Fig. 5(b) and 5(c) seem like type III, with hysteresis indicating the mesoporosity of the particle's aerogel. However, Fig. 5(a)) shows an isotherm with very distinct behavior with the adsorption step similar to type III and desorption step similar to type I [56].

Nitrogen adsorption-desorption isotherms allowed estimating the surface area (m^2/g), pore volume (cm^3/g) and average pore diameter (nm), which are presented in Table 2. The pore volume and the surface area of the aerogel were both higher (12.4-fold and 6.5-fold, respectively) than that obtained for crude corn starch, which confirms the formation of a network during the gelling process that becomes porous after sc-CO_2 drying, and the existence of mesopores inside the aerogel particles. Moreover, the surface area, pore volume and pore diameter of aerogel decreased (16.8%, 29.8%, and 11.4%, respectively) after sc-CO_2 impregnation as the β-carotene molecules partially filled the spaces formed by the porous network of the aerogels.

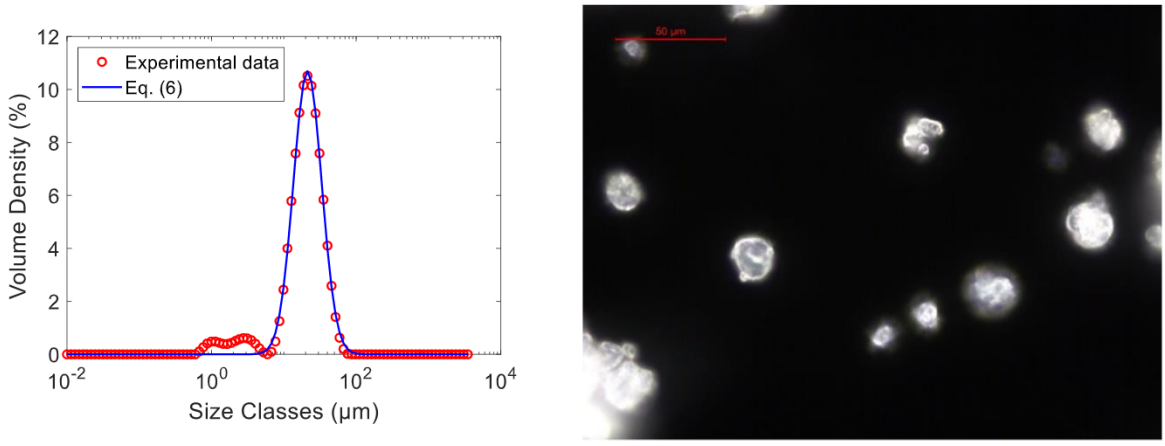

Fig. 4. (a) Particle size distribution and (b) optical microscopy image of the corn starch aerogels particles produced by sc-CO_2 drying under 12 MPa, 40 °C, and CO_2 flow rate of 10 g/min.

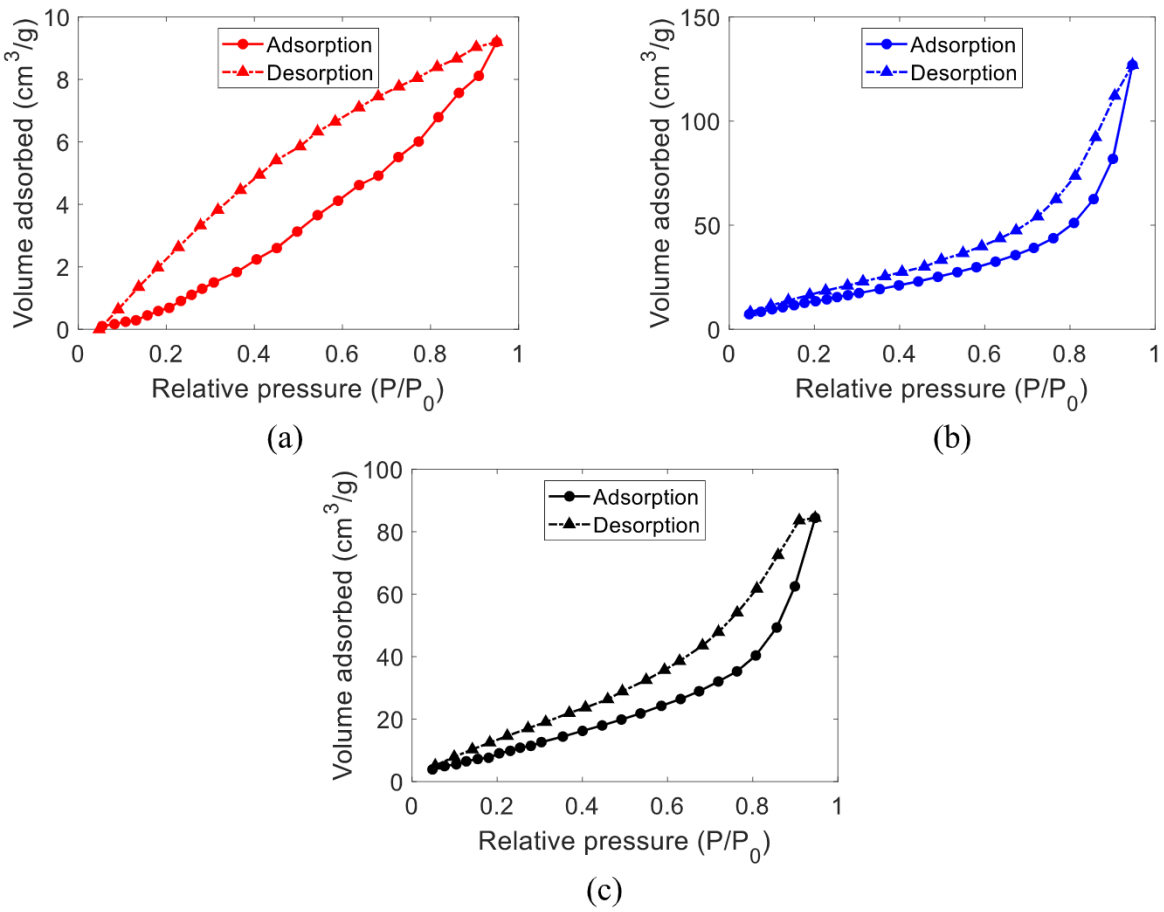

Fig. 5. Nitrogen adsorption-desorption isotherms for (a) crude corn starch; (b) corn starch aerogels produced by sc-CO_2 drying under 12 MPa, 40 °C, and CO_2 flow rate of 10 g/min; and (c) impregnated corn starch aerogel produced by sc-CO_2 impregnation under 30 MPa, 40 °C, average depressurization rate of 0.40 MPa/min, and 4 cycles.

Table 2
Physical properties of corn starch, corn starch aerogels produced by sc-CO_2 drying under 12 MPa, 40 °C and CO_2 flow rate at 10 g/min, and impregnated corn starch aerogel produced by sc-CO_2 impregnation under 30 MPa, 40 °C, average depressurization rate of 0.40 MPa/min, and 4 cycles.

Samples	A_s (m^2/g)	V_p (cm^3/g)	d_{ap} (nm)
Corn starch	9.873	0.016	n.d
Corn starch aerogel	64.320	0.198	13.044
Impregnated corn starch aerogel	53.497	0.139	11.561

A_s: surface area; V_p: Pore volume; d_{ap}: Average pore diameter.
n.d.: not determined.

The surface area of aerogels was higher than those obtained by Wang et al. [57] and lower than that observed by Dogenski et al. [58]. Although these authors also synthesized aerogels from corn starch, there are important differences related to the experimental design. Wang et al. [57], produced corn starch aerogels (monoliths) with surface area of 17.3 m^2/g, below that described in Table 2. Such difference is probably related to the use of vacuum drying. Evaporative drying, in vacuum or at ambient pressure, promotes structural collapse and consequent decrease in surface area, due to the high capillary force caused by liquid-gas surface tension and liquid-solid adhesive forces within the gel [59]. In contrast, the aerogels produced by Dogenski et al. [58] achieved a surface area of 120 m^2/g. This higher area, unlike the one observed in this work, is related to the gelatinization temperature, 90 °C. According to Mehling et al. [60], the increase in gelatinization temperature promotes greater conversion of the granular structure of starch into a fibrillar network, increasing surface area.

Similar pore volumes values (0.18 cm^3/g) were obtained by Garcia-Gonzalez et al. [61] for corn starch aerogel particles. However, this value is related to the use of high temperature, 140 °C, in the starch gelatinization process, since higher values (0.32 and 0.37 cm^3/g) were observed using temperatures of 95 °C and 120 °C, respectively. In contrast, the temperature used in this work, 75 °C, suggests that the degree of gelatinization could be improved at higher temperatures, as shown in the DSC analysis (Fig. 7). Since the maximum degree of gelatinization is not reached in the synthesis of aerogels, remaining starch granules negatively affect the network formation and thus the pore volumes [62]. On the other hand, remaining starch granules are considered resistant starches, especially those with high amylose content, and of interest for food or pharmaceutical applications [63].

Fig. 6 compares the diffractograms of crude corn starch (Fig. 6(a)), corn starch aerogels obtained by sc-CO_2 drying (Fig. 6(b)), and by sc-CO_2 impregnation with β-carotene (Fig. 6(c)). The XRD patterns of dried and impregnated aerogels both amorphous-like, which means that the supercritical drying and impregnation processes did not change the particle crystallinity. However, XRD patterns of crude starch aerogels present differences; the maxima intensity positions are different in Fig. 6 (a), which reveals changes in crystallinity during gelling. The XRD pattern indicates the crystalline part of the corn starch; peaks at 2θ, one peak at 15°, a double peak at 17°, and 18° and another peak at 23° were observed, which are following the observed by Abhari et al. [64] and Wang et al. [57]. However, these peaks disappeared in the dried and impregnated aerogels, while a new peak was observed at 20°. In accordance with these results, Wang et al. [57] observed that the characteristic peaks of native starch were substituted in corn starch

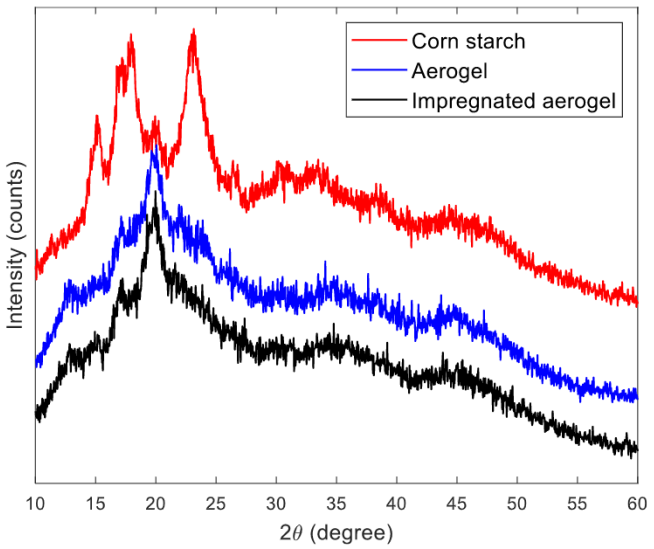

Fig. 6. X-ray diffraction (XRD) patterns for (a) crude corn starch, (b) corn starch aerogel produced by sc-CO_2 drying under 12 MPa, 40 °C, and CO_2 flow rate of 10 g/min; and (c) impregnated corn starch aerogel produced by sc-CO_2 impregnation under 30 MPa, 40 °C, average depressurization rate of 0.40 MPa/min, and 4 cycles.

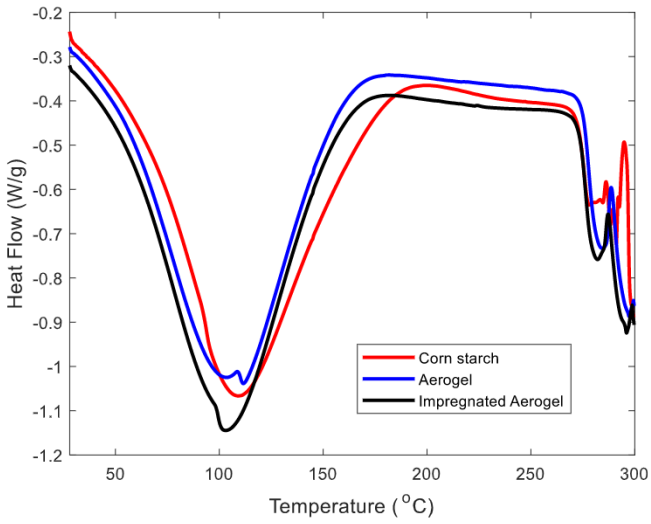

Fig. 7. DSC thermograms of crude corn starch (dotted red line), corn starch aerogel (dotted black line) produced by sc-CO_2 drying under 12 MPa, 40 °C, and CO_2 flow rate of 10 g/min, and impregnated corn starch aerogel with β-carotene (solid blue line) produced by sc-CO_2 impregnation under 30 MPa, 40 °C, average depressurization rate of 0.40 MPa/min, and 4 cycles.

aerogels by a new characteristic peak at $2\theta = 20°$. The authors attributed this new peak to the amylose-lipid complex formation that occurred by the interaction of starch and lipids through hydrophobicity when the starch was heated. Therefore, the water-in-oil emulsion produced in our work under 75 °C passed through the same phenomenon described by Wang et al. [57].

Additionally, materials that present amorphous and polyamorphic states with different solubilities and therapeutic activities are important for the transport of bioactive compounds [65]. Previously, amorphous states were not used in pharmaceutical industries due to their instability, but nowadays they are widely used [66]. In fact, most drugs have low bioavailability as they have poor water-solubility. Amorphization is classified as an effective method to enhance water-solubility and bioavailability of drugs. More information on this issue is reviewed by Shi et al. [67] and Wang et al. [68]. Accordingly, the aerogels in the current work, due to this amorphous-like behavior, are applicable for pharmaceuticals industries.

Fig. 7 shows the thermograms of crude corn starch, corn starch aerogel, and impregnated corn starch aerogel. The heat flow profile against temperature increasing almost did not differ between the three samples, except for the final region of the graphic (270–300 °C). The endothermic peak of the samples appears around 100 °C, which may be related to the starch hydrogel dehydration process.

Fig. 8 shows the FTIR spectra obtained from crude corn starch, corn starch aerogels obtained by sc-CO_2 drying, sc-CO_2 impregnation with β-carotene, and the spectrum of β-carotene standard. Similar infrared bands appear for corn starch, aerogels, and impregnated aerogels. Peaks were observed at wavelengths of approximately 3500, 1400, and 1000 cm^{-1}, being attributed to the presence of O-H, C-C, and C═O bonds in the polysaccharide structure, respectively. In addition, an isolated peak of approximately 2900 cm^{-1} was observed, corresponding C-H bonds. On the other hand, β-carotene showed peaks at wavelengths around 2900 and 900 cm^{-1}, which may be related to the C-H bonds of the linear portion of the molecule and of the aromatic ring, respectively.

From Fig. 8 one can see that corn starch, aerogel, and impregnated aerogel had similar transmittance behaviors, which may mean that the chemical composition of the aerogels did not change after supercritical drying and impregnation. Despite the use of samples of the best experimental results (0.96 mg β-carotene/g aerogel), the β-carotene loading for this analysis did not provide a significant difference in the transmittance results compared to that obtained for corn starch and aerogels.

Fig. 9 represents the morphological structure of corn starch aerogels obtained by scanning electron microscopy (SEM). Fig. 9(a) and 9(b) show the SEM images for corn starch aerogels obtained by sc-CO_2 drying under 12 MPa, 40 °C, and CO_2 flow rate of 10 g/min, and Fig. 9(c) and 7 (d) reveal impregnated corn starch aerogels with β-carotene obtained by sc-CO_2 impregnation under 30 MPa, 40 °C, average depressurization rate of 0.40 MPa/min, and 4 cycles. Fig. 9(a) and 7(c) reveal a mixture of particles of spherical and undefined shapes, and also small clusters. The heterogeneity of particle shape is possibly due to the gelation and separation steps of the corn starch particles from the emulsion [69], and the particle agglomeration may be associated with the electrostatic attraction observed after sc-CO_2 drying. In addition, Fig. 9(d) reveals the presence of a powder covering the whole sample, which may be attributed to the presence of β-carotene, while in Fig. 9(c) this phenomenon is not seen.

4. Conclusions

This work investigated the production of corn starch aerogel particles by the integration of emulsion-gelation method with sc-CO_2 drying, and sc-CO_2 impregnation of aerogels with β-carotene. The highest β-carotene loading (0.96 ± 0.07 mg β-carotene/g aerogel) was obtained at 30 MPa, 40 °C, average depressurization rate of 0.40 MPa/min and four cycles.

Thermo-physical analyses confirm amorphous and polyamorphic states of corn starch aerogels. Nitrogen adsorption-desorption graphics showed the formation of a hysteresis for the aerogel particles after sc-CO_2 drying and sc-CO_2 impregnation. The formation of a network during gelling is confirmed by the increase of the aerogel pore volume and surface area in comparison to those of crude corn starch. However, the presence of β-carotene in the samples reduced the surface area, pore volume and pore diameter of impregnated aerogels. XRD and DSC analyses, respectively, showed that crystallinity and thermal properties of the particles did not change after sc-CO_2 drying and sc-CO_2 impregnation. Moreover, FT-IR results reveal a similar behavior of the transmittance of the samples, suggesting that the chemical composition of aerogels remained unchanged. Finally, SEM images present agglomerated particles and, in some cases, powder covering the surface, being attributed to the presence of β-carotene. The main advantage of

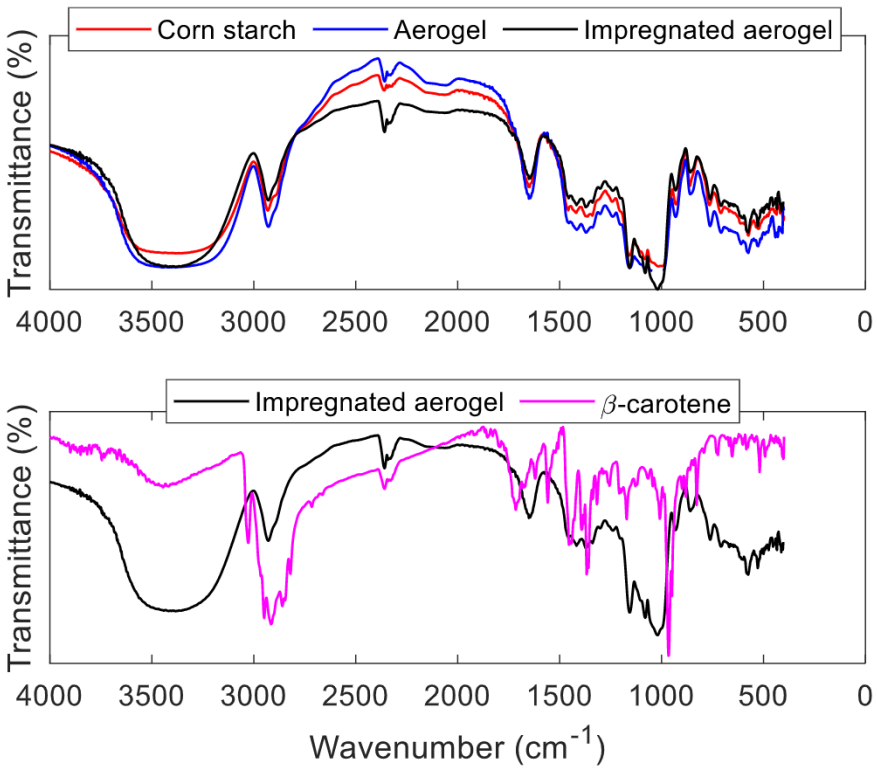

Fig. 8. FT-IR spectra of crude corn starch (red line), corn starch aerogel (blue line) produced by sc-CO_2 drying under 12 MPa, 40 °C, and CO_2 flow rate of 10 g/min, impregnated corn starch aerogel with β-carotene (black lines) produced by sc-CO_2 impregnation under 30 MPa, 40 °C, average depressurization rate of 0.40 MPa/min, and 4 cycles, and the β-carotene standard (pink line).

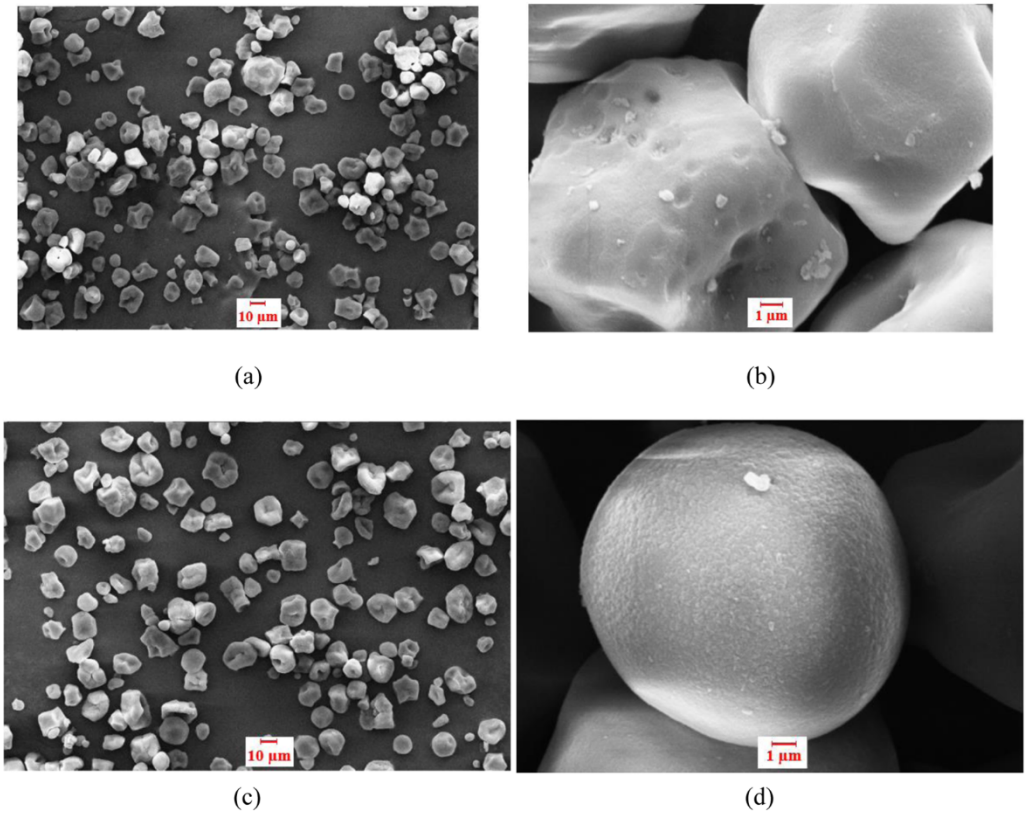

Fig. 9. Surface morphology of corn starch aerogels (a and b) produced by sc-CO_2 drying under 12 MPa, 40 °C, and CO_2 flow rate of 10 g/min, and impregnated corn starch aerogels with β-carotene (c and d) obtained by sc-CO_2 impregnation under 30 MPa, 40 °C, average depressurization rate of 0.40 MPa/min, and 4 cycles.

impregnated corn starch aerogel is that oxidation and isomerization prevention of β-carotene is expected, which can facilitate its use in food industries.

CRediT authorship contribution statement

Arthur Luiz Baião Dias: Conceptualization, Methodology, Investigation, Writing – original draft, Writing – review & editing, Funding acquisition. **Tahmasb Hatami**: Software, Formal analysis, Investigation, Writing – original draft, Writing – review & editing, Funding acquisition. **Juliane Viganó**: Conceptualization, Methodology, Investigation, Writing – original draft, Writing – review & editing, Funding acquisition. **Erick Jarles Santos de Araújo**: Writing – original draft. **Lucia Helena Innocentini Mei**: Writing – review & editing, Supervision. **Camila Alves Rezende**: Writing – review & editing, Supervision. **Julian Martínez**: Conceptualization, Writing – review & editing, Supervision, Funding acquisition.

Declaration of Competing Interest

The authors declare that they have no known competing financial interests or personal relationships that could have appeared to influence the work reported in this paper.

Acknowledgments

The authors would like to thank Conselho Nacional de Desenvolvimento Científico e Tecnológico (CNPq) [grant numbers 151005/2019-2, 408285/2018-4, 303063/2018-1], Fundação de Amparo à Pesquisa do Estado de São Paulo (FAPESP) [grant number 2017/2367-2, 2018/18722-6, 2018/23769-1 and 2020/15774-5] for financial support. This study was financed in part by the Coordenação de Aperfeiçoamento de Pessoal de Nível Superior – Brazil (CAPES) [Financial code 001].

References

[1] D.J. McClements, Y. Li, Structured emulsion-based delivery systems: controlling the digestion and release of lipophilic food components, Adv. Colloid Interface Sci. 159 (2010) 213–228.
[2] L. Mao, D. Wang, F. Liu, Y. Gao, Emulsion design for the delivery of β-carotene in complex food systems, Crit. Rev. Food Sci. 58 (2018) 770–784.
[3] Y. Wei, Z. Yu, K. Lin, C. Sun, L. Dai, S. Yang, L. Mao, F. Yuan, Y. Gao, Fabrication and characterization of resveratrol loaded zein-propylene glycol alginate-rhamnolipid composite nanoparticles: physicochemical stability, formation mechanism and in vitro digestion, Food Hydrocoll. 95 (2019) 336–348.
[4] D.B. Rodriguez-Amaya, Food Carotenoids: Chemistry, Biology and Technology, John Wiley & Sons, 2015.
[5] Y. Wei, C.X. Sun, L. Dai, X.Y. Zhan, Y.X. Gao, Structure, physicochemical stability and in vitro simulated gastrointestinal digestion properties of beta-carotene loaded zein-propylene glycol alginate composite nanoparticles fabricated by emulsification-evaporation method, Food Hydrocoll. 81 (2018) 149–158.
[6] M. Scognamiglio, I. De Marco, Supercritical CO_2 impregnation of alpha-tocopherol in different aerogels, Chem. Eng. Trans. 79 (2020) 223–228.
[7] N. Hsan, P.K. Dutta, S. Kumar, J. Koh, Arginine containing chitosan-graphene oxide aerogels for highly efficient carbon capture and fixation, J. CO2 Util. 59 (2022), 101958.
[8] B. Caballero, P. Finglas, F. Toldrá, Encyclopedia of Food and Health, Academic Press, 2015.
[9] K. Sangseethong, P. Chatakanonda, K. Sriroth, Superabsorbent hydrogels from rice starches with different amylose contents, Starch-Stärke 70 (2018) 1700244.
[10] Y. Zhang, H. Zuo, F. Xu, K. Zhu, L. Tan, W. Dong, G. Wu, The digestion mechanism of jackfruit seed starch using improved extrusion cooking technology, Food Hydrocoll. 110 (2021), 106154.
[11] S. Zhao, W.J. Malfait, N. Guerrero-Alburquerque, M.M. Koebel, G. Nyström, Biopolymer aerogels and foams: chemistry, properties, and applications, Angew. Chem. Int. Ed. 57 (2018) 7580–7608.
[12] F. Zhu, Starch based aerogels: production, properties and applications, Trends Food Sci. Technol. 89 (2019) 1–10.
[13] L. Goimil, M.E.M. Braga, A.M.A. Dias, J.L. Gomez-Amoza, A. Concheiro, C. Alvarez-Lorenzo, H.C. de Sousa, C.A. Garcia-Gonzalez, Supercritical processing of starch aerogels and aerogel-loaded poly (epsilon-caprolactone) scaffolds for sustained release of ketoprofen for bone regeneration, J. Co2 Util. 18 (2017) 237–249.
[14] R.P. Ellis, M.P. Cochrane, M.F.B. Dale, C.M. Duffus, A. Lynn, I.M. Morrison, R.D. M. Prentice, J.S. Swanston, S.A. Tiller, Starch production and industrial use, J. Sci. Food Agric. 77 (1998) 289–311.
[15] H. Kargarzadeh, J. Huang, N. Lin, I. Ahmad, M. Mariano, A. Dufresne, S. Thomas, A. Gałęski, Recent developments in nanocellulose-based biodegradable polymers, thermoplastic polymers, and porous nanocomposites, Prog. Polym. Sci. 87 (2018) 197–227.
[16] Q. Zheng, Y. Tian, F. Ye, Y. Zhou, G. Zhao, Fabrication and application of starch-based aerogel: technical strategies, Trends Food Sci. Technol. 99 (2020) 608–620.
[17] M. Sjöö, L. Nilsson, Starch in Food: Structure, Function and Applications, Woodhead Publishing, 2017.
[18] Y. Wang, Y. Su, W. Wang, Y. Fang, S.B. Riffat, F. Jiang, The advances of polysaccharide-based aerogels: preparation and potential application, Carbohydr. Polym. 226 (2019), 115242.
[19] C.A. García-González, M. Jin, J. Gerth, C. Alvarez-Lorenzo, I. Smirnova, Polysaccharide-based aerogel microspheres for oral drug delivery, Carbohydr. Polym. 117 (2015) 797–806.
[20] D. Weber, T. Grune, The contribution of β-carotene to vitamin A supply of humans, Mol. Nutr. Food Res. 56 (2012) 251–258.
[21] N. Ganan, M.G. Bordon, P.D. Ribotta, A. Gonzalez, Study of chia oil microencapsulation in soy protein microparticles using supercritical Co-2-assisted impregnation, J. Co2 Util. 40 (2020).
[22] P. Franco, L. Incarnato, I. De Marco, Supercritical CO_2 impregnation of alpha-tocopherol into PET/PP films for active packaging applications, J. Co2 Util. 34 (2019) 266–273.
[23] J.E. Mosquera, M.L. Goni, R.E. Martini, N.A. Ganan, Supercritical carbon dioxide assisted impregnation of eugenol into polyamide fibers for application as a dental floss, J. Co2 Util. 32 (2019) 259–268.
[24] M. Champeau, J.M. Thomassin, T. Tassaing, C. Jerome, Drug loading of polymer implants by supercritical CO_2 assisted impregnation: a review, J. Control Release 209 (2015) 248–259.
[25] S. Milovanovic, D. Markovic, K. Aksentijevic, D.B. Stojanovic, J. Ivanovic, I. Zizovic, Application of cellulose acetate for controlled release of thymol, Carbohydr. Polym. 147 (2016) 344–353.
[26] Y. He, X. Hou, J. Guo, Z. He, T. Guo, Y. Liu, Y. Zhang, J. Zhang, N. Feng, Activation of a gamma–cyclodextrin–based metal–organic framework using supercritical carbon dioxide for high–efficient delivery of honokiol, Carbohydr. Polym. 235 (2020), 115935.
[27] P. Franco, I. De Marco, Supercritical CO_2 adsorption of non-steroidal anti-inflammatory drugs into biopolymer aerogels, J. Co2 Util. 36 (2020) 40–53.
[28] A. Ubeyitogullari, O.N. Ciftci, Generating phytosterol nanoparticles in nanoporous bioaerogels via supercritical carbon dioxide impregnation: effect of impregnation conditions, J. Food Eng. 207 (2017) 99–107.
[29] A. Rojas, A. Torres, M.J. Galotto, A. Guarda, R. Julio, Supercritical impregnation for food applications: a review of the effect of the operational variables on the active compound loading, Crit. Rev. Food Sci. 60 (2020) 1290–1301.
[30] Y.D. Sun, Supercritical fluid particle design for poorly water-soluble drugs (review), Curr. Pharm. Des. 20 (2014) 349–368.
[31] M. Banchero, L. Manna, S. Ronchetti, P. Campanelli, A. Ferri, Supercritical solvent impregnation of piroxicam on PVP at various polymer molecular weights, J. Supercrit. Fluids 49 (2009) 271–278.
[32] M. Belizón, M. Fernández-Ponce, L. Casas, C. Mantell, E.M. De La Ossa-Fernández, Supercritical impregnation of antioxidant mango polyphenols into a multilayer PET/PP food-grade film, J. CO2 Util. 25 (2018) 56–67.
[33] P. Franco, B. Aliakbarian, P. Perego, E. Reverchon, I. De Marco, Supercritical adsorption of quercetin on aerogels for active packaging applications, Ind. Eng. Chem. Res. 57 (2018) 15105–15113.
[34] G.R. Medeiros, S.R. Ferreira, B.A. Carciofi, High pressure carbon dioxide for impregnation of clove essential oil in LLDPE films, Innov. Food Sci. Emerg. Technol. 41 (2017) 206–215.
[35] A. Rojas, D. Cerro, A. Torres, M.J. Galotto, A. Guarda, J. Romero, Supercritical impregnation and kinetic release of 2-nonanone in LLDPE films used for active food packaging, J. Supercrit. Fluids 104 (2015) 76–84.
[36] C. Villegas, A. Torres, M. Rios, A. Rojas, J. Romero, C.L. de Dicastillo, X. Valenzuela, M.J. Galotto, A. Guarda, Supercritical impregnation of cinnamaldehyde into polylactic acid as a route to develop antibacterial food packaging materials, Food Res. Int. 99 (2017) 650–659.
[37] A.C. de Souza, A.M. Dias, H.C. Sousa, C.C. Tadini, Impregnation of cinnamaldehyde into cassava starch biocomposite films using supercritical fluid technology for the development of food active packaging, Carbohydr. Polym. 102 (2014) 830–837.
[38] C. Cejudo-Bastante, P. Arjona-Mudarra, M.T. Fernández-Ponce, L. Casas, C. Mantell, E.J. Martínez de la Ossa, C. Pereyra, Application of a natural antioxidant from grape pomace extract in the development of bioactive jute fibers for food packaging, Antioxidants 10 (2021) 216.
[39] I. De Marco, E. Reverchon, Starch aerogel loaded with poorly water-soluble vitamins through supercritical CO_2 adsorption, Chem. Eng. Res. Des. 119 (2017) 221–230.
[40] M. Villegas, A.L. Oliveira, R.C. Bazito, P. Vidinha, Development of an integrated one-pot process for the production and impregnation of starch aerogels in supercritical carbon dioxide, J. Supercrit. Fluids 154 (2019), 104592.
[41] I. De Marco, R. Iannone, S. Miranda, S. Riemma, An environmental study on starch aerogel for drug delivery applications: effect of plant scale-up, Int. J. Life Cycle Assess. 23 (2018) 1228–1239.
[42] T. Hatami, J. Vigano, L.H.I. Mei, J. Martinez, Production of alginate-based aerogel particles using supercritical drying: experiment, comprehensive mathematical model, and optimization, J. Supercrit. Fluids 160 (2020), 104791.
[43] R.L. Mendes, B.P. Nobre, J.P. Coelho, A.F. Palavra, Solubility of β-carotene in supercritical carbon dioxide and ethane, J. Supercrit. Fluids 16 (1999) 99–106.

[44] P. dos Santos, C.A. Rezende, J. Martínez, Activity of immobilized lipase from Candida antarctica (Lipozyme 435) and its performance on the esterification of oleic acid in supercritical carbon dioxide, J. Supercrit. Fluids 107 (2016) 170–178.
[45] A.L.B. Dias, G.N. da Cunha, P. dos Santos, M.A.A. Meireles, J. Martinez, Fusel oil: water adsorption and enzymatic synthesis of acetate esters in supercritical CO_2, J. Supercrit. Fluids 142 (2018) 22–31.
[46] M.L. Goni, N.A. Ganan, S.E. Barbosa, M.C. Strumia, R.E. Martini, Supercritical CO_2-assisted impregnation of LDPE/sepiolite nanocomposite films with insecticidal terpene ketones: Impregnation yield, crystallinity and mechanical properties assessment, J. Supercrit. Fluid 130 (2017) 337–346.
[47] M.L. Goni, N.A. Ganan, J.M. Herrera, M.C. Strumia, A.E. Andreatta, R.E. Martini, Supercritical CO_2 iof LDPE films with terpene ketones as biopesticides against corn weevil (Sitophilus zeamais), J. Supercrit. Fluid 122 (2017) 18–26.
[48] V.S. Carvalho, A.L.B. Dias, K.P. Rodrigues, T. Hatami, L.H.I. Mei, J. Martínez, J. Viganó, Supercritical fluid adsorption of natural extracts: technical, practical, and theoretical aspects, J. CO2 Util. 56 (2022), 101865.
[49] M. Johannsen, G. Brunner, Solubilities of the fat-soluble vitamins A, D, E, and K in supercritical carbon dioxide, J. Chem. Eng. Data 42 (1997) 106–111.
[50] H. Sovová, R.P. Stateva, A.A. Galushko, Solubility of β-carotene in supercritical CO_2 and the effect of entrainers, J. Supercrit. Fluids 21 (2001) 195–203.
[51] I. Pasquali, J.M. Andanson, S.G. Kazarian, R. Bettini, Measurement of CO_2 sorption and PEG 1500 swelling by ATR-IR spectroscopy, J. Supercrit. Fluid 45 (2008) 384–390.
[52] B. Bonavoglia, G. Storti, M. Morbidelli, A. Rajendran, M. Mazzotti, Sorption and swelling of semicrystalline polymers in supercritical CO_2, J. Polym. Sci. Pol. Phys. 44 (2006) 1531–1546.
[53] Z.G. Lei, H. Ohyabu, Y. Sato, H. Inomata, R.L. Smith, Solubility, swelling degree and crystallinity of carbon dioxide-polypropylene system, J. Supercrit. Fluid 40 (2007) 452–461.
[54] A.A. Escobar-Puentes, S.Y. Reyes-Lopez, A.D.R. Baltazar, V. Lopez-Teros, A. Wall-Medrano, Molecular interaction of beta-carotene with sweet potato starch: a bleaching-restitution assay, Food Hydrocoll. 127 (2022).
[55] H.G. Merkus, Particle Size Measurements: Fundamentals, Practice, Quality, Springer Science & Business Media, 2009.
[56] M. Ben Yahia, Y. Ben Torkia, S. Knani, M.A. Hachicha, M. Khalfaoui, A. Ben, Lamine, models for Type VI adsorption isotherms from a statistical mechanical formulation, Adsorpt. Sci. Technol. 31 (2013) 341–357.
[57] Y.W. Wang, M.H. He, Y.W. Wu, Y.G. Liu, J. Ouyang, Effect of crosslinking agents on the physicochemical and digestive properties of corn starch aerogel, Starch-Starke 73 (2021).
[58] M. Dogenski, H.J. Navarro-Diaz, J.V. de Oliveira, S.R.S. Ferreira, Properties of starch-based aerogels incorporated with agar or microcrystalline cellulose, Food Hydrocoll. 108 (2020).
[59] G.W. Scherer, Stress in aerogel during depressurization of autoclave: I. Theory, J. Sol-Gel Sci. Technol. 3 (1994) 127–139.
[60] T. Mehling, I. Smirnova, U. Guenther, R.H.H. Neubert, Polysaccharide-based aerogels as drug carriers, J. Non Cryst. Solids 355 (2009) 2472–2479.
[61] C.A. Garcia-Gonzalez, J.J. Uy, M. Alnaief, I. Smirnova, Preparation of tailor-made starch-based aerogel microspheres by the emulsion-gelation method, Carbohydr. Polym. 88 (2012) 1378–1386.
[62] G.M. Glenn, D.W. Irving, Starch-based microcellular foams, Cereal Chem. 72 (1995) 155–161.
[63] H.T. Li, M.J. Gidley, S. Dhital, High-amylose starches to bridge the “fiber gap”: development, structure, and nutritional functionality, Compr. Rev. Food Sci. Food Saf. 18 (2019) 362–379.
[64] N. Abhari, A. Madadlou, A. Dini, Structure of starch aerogel as affected by crosslinking and feasibility assessment of the aerogel for an anti-fungal volatile release, Food Chem. 221 (2017) 147–152.
[65] J. Bauer, S. Spanton, R. Henry, J. Quick, W. Dziki, W. Porter, J. Morris, Ritonavir: an extraordinary example of conformational polymorphism, Pharm. Res. 18 (2001) 859–866.
[66] P. Gurikov, I. Smirnova, Amorphization of drugs by adsorptive precipitation from supercritical solutions: a review, J. Supercrit. Fluid 132 (2018) 105–125.
[67] Q. Shi, F. Li, S. Yeh, S.M. Moinuddin, J.B. Xin, J. Xu, H. Chen, B. Ling, Recent advances in enhancement of dissolution and supersaturation of poorly water-soluble drug in amorphous pharmaceutical solids: a review, Aaps Pharmscitech 23 (2021).
[68] B. Wang, F.L. Liu, J. Xiang, Y.J. He, Z.B. Zhang, Z.N. Cheng, W.J. Liu, S.W. Tan, A critical review of spray-dried amorphous pharmaceuticals: synthesis, analysis and application, Int. J. Pharm. 594 (2021).
[69] M. Alnaief, M. Alzaitoun, C. García-González, I. Smirnova, Preparation of biodegradable nanoporous microspherical aerogel based on alginate, Carbohydr. Polym. 84 (2011) 1011–1018.